\Carboxylated Chitosan Nanocrystals: Novel Synthetic Route and Application as Superior Support for Gold-Catalyzed Reactions

Tony Jin[a], Davis Kurdyla[a,b], Sabahudin Hrapovic[b], Alfred C.W. Leung[b], Sophie Régnier[b], Yali Liu[b], Audrey Moores*[,a,c] and Edmond Lam*[,b]

[a]Department of Chemistry, McGill University, 801 Sherbrooke St. West, Montreal, Quebec, H3A 0B8 Canada
[b]Aquatic and Crop Resource Development Research Centre, National Research Council of Canada, 6100 Royalmount Avenue, Montreal, Quebec, H4P 2R2 Canada
[c]Department of Materials Engineering, McGill University, 3610 University Street, Montreal, Quebec H3A 0C5, Canada

KEYWORDS: Chitosan, biomass, nanocrystal, heterogeneous catalysis, gold nanoparticle, coupling, catalyst support, chitin

Abstract

Chitin nanocrystals (ChNCs) were prepared by partial cleavage of glycosidic bonds in chitin with concurrent oxidation of chitin C6 primary alcohols to produce carboxylate groups on the surface of the ChNCs. Following alkaline deacetylation of the ChNCs in the presence of $NaBH_4$ to inhibit “end-peeling” afforded chitosan nanocrystals (ChsNCs) with a degree of deacetylation (DDA) >80%. Transmission electron microscopy (TEM), X-ray diffraction (XRD) and Fourier-transform Infrared (FTIR) spectroscopy were used to determine the morphology and composition of these carboxylated ChNCs and ChsNCs. Subsequently, two methods were used to deposit Au onto the nanocrystals, and the catalytic activities of the resulting biomass-based nanocatalysts were tested for the 4-nitrophenol reduction and the aldehyde-amine-alkyne (A^3) coupling reaction. In particular, Au nanoparticles over ChsNCs featured the highest turnover frequency value for the 4-nitrophenol reduction reported to date. Spectroscopic and imaging techniques confirmed the importance of controlling precisely the redox state of Au as it is being deposited to afford highly disperse active site on the bio-nano-support.

Introduction

Research into bio-based nanomaterials has seen major advancements in the past decade for a multitude of disciplines ranging from energy, electronics, medicine, sustainable packaging, environmental remediation, and coatings.[1-3] This effort was pioneered by research on cellulose nanocrystals (CNCs), a material readily accessible via cellulose acid hydrolysis. CNCs are non-toxic materials with large surface area, high mechanical strength, and tunable colloidal and self assembly behaviour in aqueous media, making them suitable for a number of downstream applications in nanomedicinal drug delivery, food packaging, or papermaking industry, to name only a few.[4-7] Their small size and the presence of coordinating groups on their surface, such as hydroxyls, sulfate half esters and carboxylates, make them ideal candidates for the stabilization of metal nanoparticles (NPs), which have been further utilized in catalysis.[8-14] In particular it was shown that CNCs were excellent stabilizers for Au NPs applied to nitrophenol reduction, Ru NPs for arene hydrogenation, Ag for carbonyl hydrogenation, Pd for phenol hydrogenation and even for highly effective chirality transfer from the CNC surface in a Pd-catalyzed carbonyl hydrogenation reaction.[9, 15-18]

While cellulose in its nanocrystalline form was undergoing these exciting developments, chitin, on the other hand, had been scarcely explored in this form, despite the presence of nitrogen-containing functionalities as a handle for further manipulations.[19] Chitin serves as a core structural material in crustaceans, fungi, and certain insects, in a similar manner to cellulose for trees and plants. With shrimp and crab shells as primary sources, the annual availability of chitin is in the range of 1 to 100 billion tons.[20] Currently in the seafood

industry, shell waste is often discarded back into the sea or in landfills, causing disposal costs as well as environmental concerns.[21] Crustacean shells are mostly composed of proteins, calcium carbonate and chitin, which are all potential sources of valuable chemicals and the basis for a “shell biorefinery,” analogous to the forestry biorefinery where conversion processes and equipment are integrated to produce fuels, power, heat, and value-added chemicals from lignocellulosic biomass.[22] Challenges to establishing a shell biorefinery including the sustainable fractionation processes to separate the components of shell waste, to establish chemical methods to produce value-added chemicals, and to identify downstream applications for these materials that lead to consumer products.[23]

Chitin possesses a number of perceived beneficial properties for downstream applications including high bioavailability, antimicrobial properties, and high tensile strength. However, its limited solubility in aqueous and organic media have constrained actual deployment of chitin in applications.[24-28] In lieu of this, the increased solubility of chitosan and its amino functional groups leads to greater reactivity compared to chitin in applications development, yet green methods for the conversion of chitin into chitosan are still highly sought after.[26, 28] Chitosan has been reported as a bio-based support for metal NPs for use in catalysis.[29-32] However, in order to increase surface area and affinity for binding ability to metals, chitosan should be processed into nanoscale dimensions like CNCs so as to maximize the potential of this biomaterial. The production of chitin nanocrystals (ChNCs) and related chitin nanofibrils is known.[33-35] Typically, strong mineral acids are used to hydrolyze the amorphous regions of chitin to yield highly

crystalline nano-chitin materials. In another case, Isogai and co-workers used TEMPO-mediated oxidation to produce carboxylated chitin nanofibrils.[33] However these methods rely on the use of harsh and/or corrosive chemicals. Our group (Lam) has recently patented the procedure for producing carboxylated ChNCs from chitin using ammonium persulfate as a mild oxidant,[36] and other groups have followed suited and used similar methods.[37-39] From ChNCs, a major goal is the formation of chitosan nanocrystals (ChsNCs) by deacetylation, since the amine functionalities will impart surface charges to the nanocrystals and thus improve dispersibility in polar solvents. We (Lam group) reported that the use of concentrated NaOH to directly deacetylate ChNCs does lead to the formation of ChsNCs.[36] However, the process had severe limitations as attempts to further deacetylate ChNCs above 70% degree of deacetylation (DDA) leads to uncontrolled depolymerization of the chitin structure, resulting in the production of spherical NPs with non-uniform size distribution. A challenge exists in fabricating ChsNCs with the expressed goals of creating biomaterials with high DDA, retention of nano-rod structure to minimize aggregation, and uniform size distribution to minimize un-necessary downstream separation steps. Aside from the development of clean ChNCs and ChsNCs syntheses, hybridization of ChNCs and ChsNCs with metal NPs remains largely unexplored, despite the expected advantages of nitrogen-containing groups presence at their surface as compared to their CNCs counterparts, in particular in terms of long-term stability and chemical reactivity. Herein, we first provide a facile and scalable procedure for fabricating carboxylated ChNCs and ChsNCs from chitin. After physicochemical characterization, two methods were then used to immobilize Au onto both carboxylated ChNCs and ChsNCs. Au NPs were selected as our initial targeted catalyst material due

to its relatively low toxicity, along with having heightened catalytic ability for specific reactions such as the reduction of olefins and nitro-containing compounds.[40] ChsNC-supported Au was tested as catalysts for the reduction of 4-nitrophenol and for the aldehyde-amine-alkyne (A^3) coupling reaction. For the reduction of 4-nitrophenol, we observed the highest turnover frequencies (TOFs) ever reported, and suggest that this high activity is caused by the high dispersibility of the Au NPs on ChsNCs as a support. For the A^3 coupling reaction, it was found that high activity was linked to the ability of ChsNCs to effectively stabilize highly disperse Au in the +1 oxidation state. We hope to provide an initial framework for the design and synthesis of carboxylated ChsNCs, as well as demonstrate the remarkable applicability that this biomass material has in stabilizing active metal species for other catalyst systems.

Results and Discussion

Synthesis of ChNCs and ChsNCs

The synthesis of nano-polysaccharides (CNCs and ChNCs) typically use high concentrations of strong acids (H_2SO_4 or HCl), where hydrolysis occurs through protonation of the glycosidic oxygen units in the biopolymeric chain, yielding fragments of shorter chain biopolymers while preserving the glucopyranosic backbone.[41, 42] It is accepted that amorphous regions in native cellulose or chitin are more accessible to acidic hydrolysis attack, leaving the crystalline regions intact. We have demonstrated that dilute solutions of ammonium persulfate (APS) could act as green reagents to afford similar selective hydrolysis reactions with either cellulose or chitin.[36, 43] Specifically, in acidic media, persulfate radicals along with hydrogen peroxide are released and act in

concert to degrade the amorphous regions of the biopolymer chain, via free-radical propagation and oxidation of the glycosidic bond. The oxidative environment also explains the oxidation of surface primary alcohol functionalities into carboxylic acids.[43]

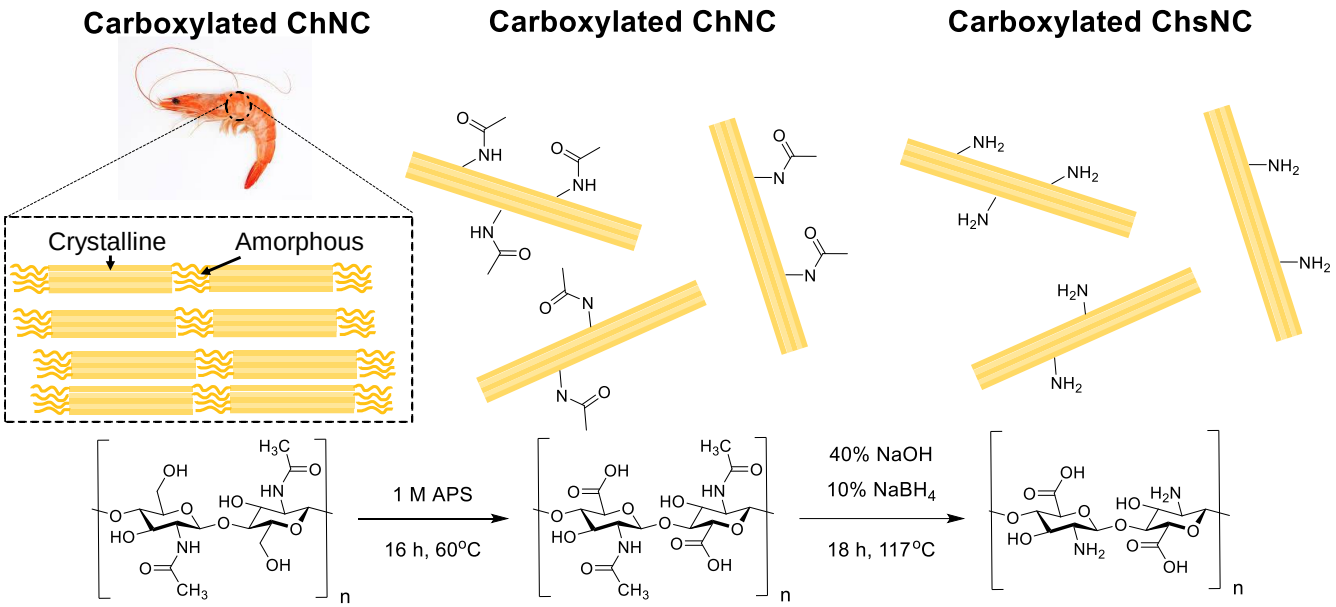

Scheme 1: Schematic depicting the two steps of fabrication from bulk chitin to carboxylated chitosan nanocrystals

Bulk chitin from shrimp shells were treated with APS at 60°C for 16 h to afford carboxylated ChNCs as shown in Scheme 1. The ChNC morphology was analyzed by low voltage TEM (LV-TEM, Figure 1a). The average size of the nanorod ChNCs is 239 ± 7 nm in length, and 4.60 ± 0.06 nm in width (n=400). AFM images confirmed these results (Figure S1a). FTIR analysis of ChNCs (Figure 1c) was used to identify the chemical transformations caused by APS treatment (full assignment in Table S1). Overall, FTIR spectra of bulk chitin (blue line) and synthesized ChNCs (orange line) are similar, with the exception of a peak centred at 1743 cm^{-1} present only in ChNC, attributed to the C=O stretching band. It confirmed that chitin C6 alcohols were oxidized into carboxylic acids in

ChNCs (Figure 1c, Figure S2). Bulk chitin and ChNCs were characterized by X-ray diffraction (XRD - Figure 1d). Characteristic diffraction peaks located at 9.6°, 19.6°, 21.1° and 23.7° are consistent α-chitin polymorph for ChNCs.[44-46] The crystallinity index (CRI) of ChNCs was estimated to be 75.9%, similar to bulk α-chitin of 82.2%.[47] This result is comparable to other crystalline chitin nanomaterials, such as an 86% literature value reported for chitin nanowhiskers.[48]

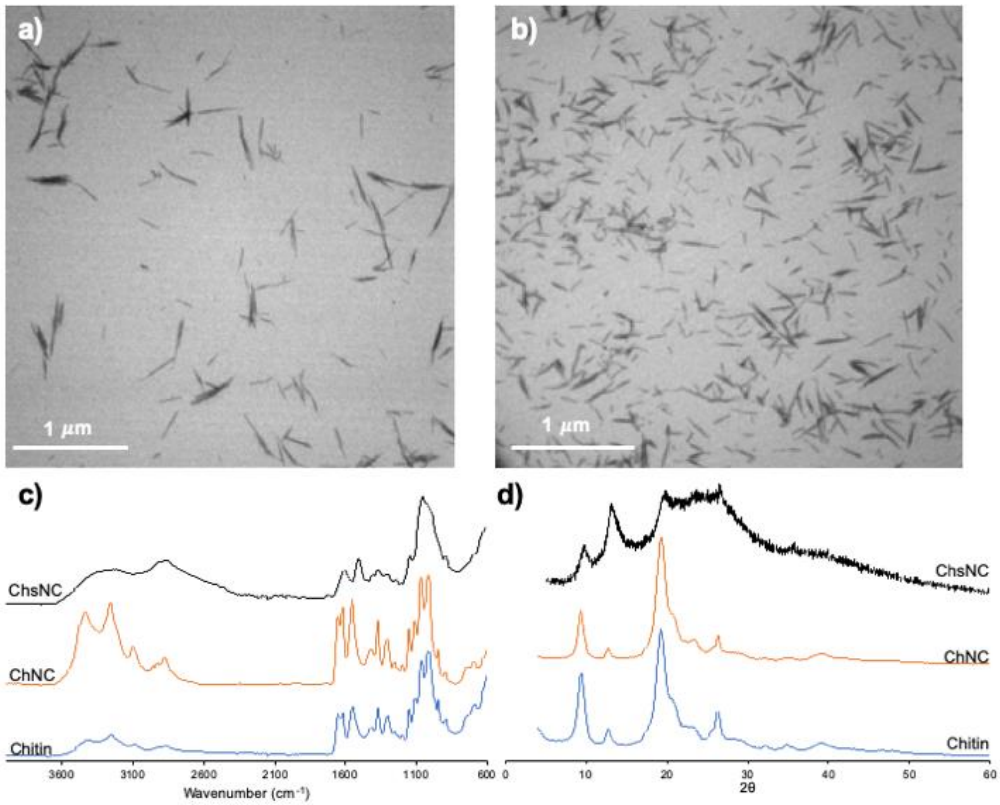

Figure 1 LV-TEM micrographs taken at 5600× magnification of (a) ChNCs and (b) ChsNCs. (c) FTIR spectra of bulk chitin (blue), ChNCs (orange), and ChsNCs (black). (d) XRD spectra of bulk chitin, ChNCs, and ChsNCs.

In order to deacetylate ChNCs into ChsNCs, ChNCs were suspended into a 40% (w/w) aqueous solution of NaOH at 117 ^{o}C for 18 h. Novel to this report is the addition of 10%

(w/w) $NaBH_4$ as a crucial reagent to prevent depolymerization previously reported.[36] This method has been developed to control the similar "end-peeling" phenomenon of cellulosic materials in alkaline environments.[49] Specifically, $NaBH_4$ selectively reduces the terminal alditols of the polymer chains.[50] LV-TEM analysis of ChsNCs confirmed the desired retention of nano-rod structure across the sample (Figure 1b), where the average size of the ChsNC is 182 $\pm$ 2 nm in length and 2.68 $\pm$ 0.02 nm in width (n=1048), with further evidence in the AFM imaging (Figure S1b). Retention of the carboxylic acid COOH stretch is apparent in FTIR (Figure 1c), which validates that $NaBH_4$ does not reduce the carboxylic acid functionality in the process. It is noted though that spectral features within the peaks are lost in the FTIR spectrum of ChsNCs in comparison to both ChNCs and bulk chitin, notably in the O-H and N-H stretching peaks in the 3500–3000 cm^{-1} region (Table S1). This phenomenon is attributed to a loss of crystallinity within the ChsNCs. The amide peak intensities found at 1560 cm^{-1} and 1030 cm^{-1} can be used to determine the DDA using a previously reported method.[33, 51] In all cases, the DDA was measured to be higher than 80% for ChsNCs. In contrast, in the absence of methods to control end-peeling, the direct deacetylation of ChNCs to ChsNCs led to the formation of variably-sized, spherical chitosan NPs, which can be seen in both AFM (Figure S1c) and TEM (Figure S3).

XRD analysis confirmed ChsNCs (Figure 1d) were amorphized during deacetylation treatment, in agreement with the FTIR data (Figure 1c). The CRI value for ChsNCs was estimated to be 23.6%, a major decrease from 75.9% measured for ChNCs. This crystallinity decrease was accompanied by a small shift towards higher angles and a large

intensity decrease of the 020 reflection at 9.6°. A similar, yet much more intense, shift of this peak all the way to 11° had been previously reported by Chirachanchai and was associated with the formation of a webbed scaffold, distinct from the discreet crystals we observed for ChsNC.[52] Also, previous studies reported that the decrease in intensity of the 020 reflection correlated linearly with DDA value.[53] The peak at 12.5° is attributed to the 021 reflection and remained fairly intense as chitin was converted from ChNCs to ChsNCs, although a direct comparison between peaks intensity is misleading because of the large difference in signal-to-noise ratios in the various XRD spectra. Interestingly for the ChsNCs XRD spectrum, a high degree of convolution is seen in the reflections that envelope the chitin peaks found at 19.6°, 21.1° and 23.7°, which are the 110, 120 and 101 reflections, respectively, as a consequence of amorphization. Similar amorphization effects were observed in many other chitin to chitosan deacetylation procedures.[53, 54]

DLS and ζ potential measurements were also conducted for both ChNCs and ChsNCs and presented in Table 1. The negative ζ potential value of -36.9 ± 3.1 mV for ChNCs in water is consistent with the presence of negatively charged carboxylate groups at the nanorod surface. Conversely, a positive value of 47.3 ± 1.0 mV for the ζ potential is indicative of the positive surface charge on ChsNCs from the protonated amino groups dispersed in water at pH ~6.5.

Table 1: DLS and ζ potential measurements of ChNCs and ChsNCs at pH 6.5

Sample	Apparent Particle Size (nm)	Polydispersity Index (PDI)	Ζ Potential (mV)
ChNC	99.0 ± 1.9	0.189 ± 0.016	-36.9 ± 3.1
ChsNC	149.8 ± 0.3	0.187 ± 0.004	+47.3 ± 1.0

As both amines and carboxylates are pH active functional groups, the pH-responsive behaviour of ChsNCs was investigated by using DLS and ζ potential measurements and compared with bulk chitosan (Figure S4).[55] Different concentrations of ChsNCs in acetic acid were prepared in the range 1-0.1% (w/w) and the pH was adjusted from 1-12 by adding either HCl or NaOH solutions. At pH 2, ChsNC amino groups are protonated, resulting in dispersed ChsNC solutions with positive ζ potentials beyond 50 mV. As the pH was decreased to under pH 2, a decrease in the absolute value of the ζ potential was reported, likely because of the high ionic charge resulting from the strong HCl concentrations in these conditions, resulting in surface charge shielding. As the pH of the ChsNC solutions was increased from 2 to 7, the absolute value of the ζ potential decreased steadily to <20 mV, consistent with the gradual deprotonation of the quaternary ammonium groups. As the solutions became very basic (pH >10), the ζ potential dropped below 0 mV to a few units mV in the negative scale, revealing the negative charges of the carboxylate groups. The apparent particle size was measured by DLS. Under acidic conditions and up to pH 6.5, the apparent particle size of ChsNCs remained constant around 120 nm, a value consistent with AFM and TEM measurements. Beyond 6.5 though, the particle size increased rapidly as a function of pH, as a result of the drop in surface charge. This justifies that acidic conditions were kept while exploring the properties of ChsNCs for catalysis in the following.

The physicochemical characterization of the carboxylated ChsNCs confirmed that the developed process afforded crystalline, nanorod-shaped ChsNCs with DDA consistently above 80%. The scalability of the process presented in Scheme 1 has been demonstrated in which ChNCs have been produced at the 200 L batch scale, while ChsNCs have been produced at the 5 L batch scale, as shown in the supporting information.

Deposition of Au onto ChNCs and ChsNCs

We then explored the use of these nanoscale biomaterials as supports for Au NPs owing to their unique chemical functionalities and higher overall surface area compared to their bulk counterparts. In order to pave the way as initial frameworks for metal NP deposition onto ChsNCs domains, two separate strategies of Au NP immobilization were investigated as outlined in Scheme 2.

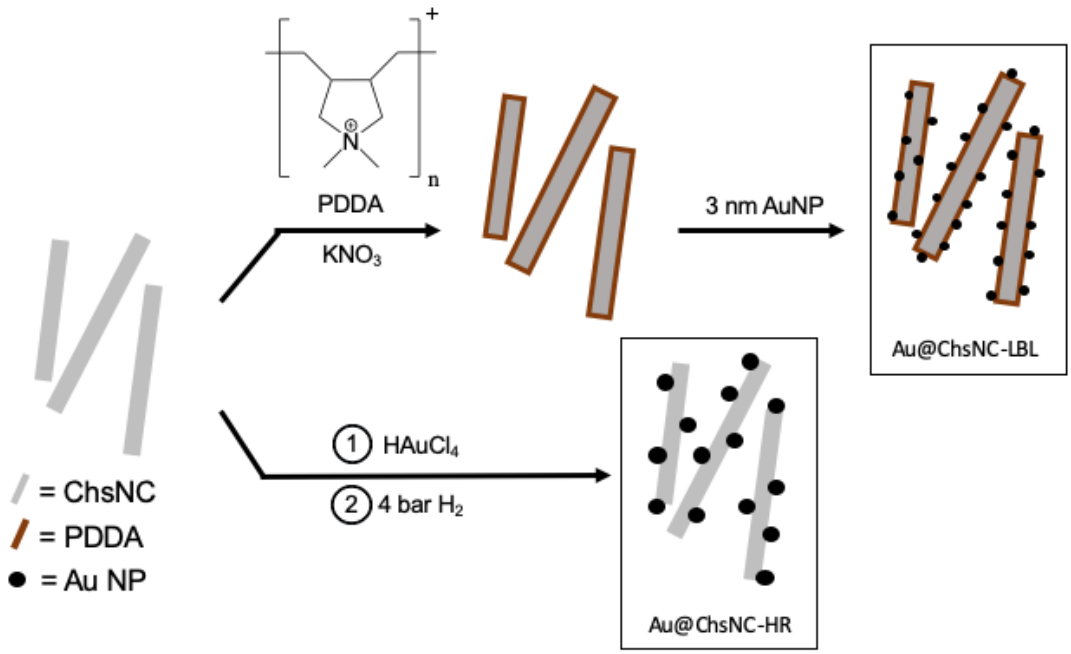

Scheme 2: Synthetic routes to deposit Au NPs onto the ChsNCs. The two fabrication routes presented are the layer-by-layer method (LBL, top) and hydrogen reduction method (HR, bottom).

The first method investigated the "layer-by-layer" (LBL) method, a two-step process previously developed by Lam et. al for CNC functionalization.[18] This method enables the immobilization of pre-fabricated, carbonate-stabilized Au NPs of small size (<5 nm) onto CNCs. The positively charged polymer poly(diallyldimethylammonium) PDDA was coated onto ChsNCs, before Au NPs were immobilized over this hybrid, resulting in the formation of a light purple solid, Au@ChsNC-LBL. TEM imaging (Figure 2a) showed Au NPs deposited onto ChsNC with an average size of 3.7 ± 0.8 nm (Figure S5) with many of them aggregated in discrete locations along the nanorods. UV-Vis absorption

corroborated this aggregation (Figure S6). A red shift of the localized surface plasmon resonance (LSPR) peak of the ready-made 3 nm Au NPs at 510 nm to 525 nm for Au@ChsNC-LBL was observed, which is a well-known effect of aggregation.[56,57]

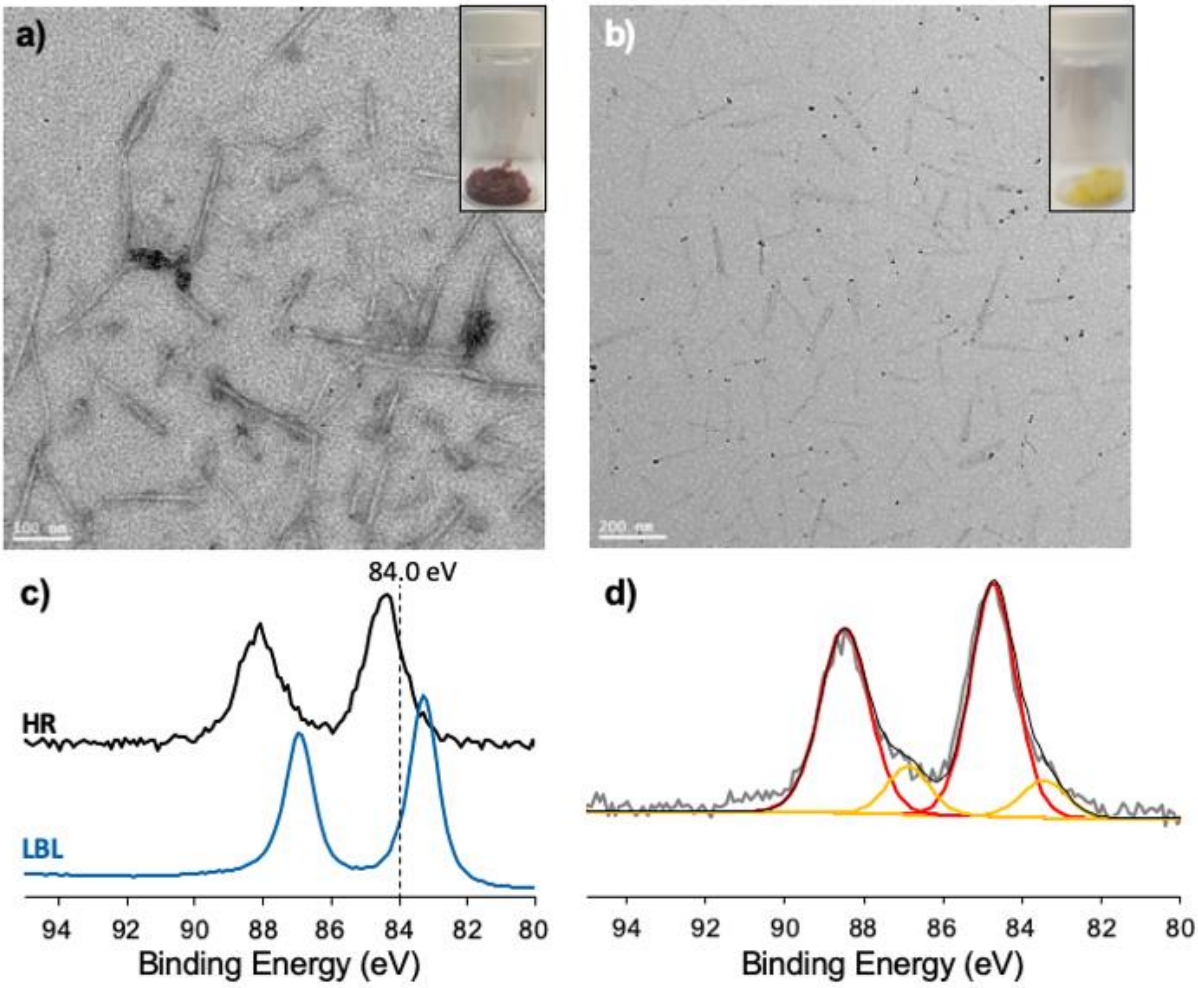

Figure 2 Brightfield TEM micrographs at 25000× magnification for (a) Au@ChsNC-LBL and (b) Au@ChsNC-HR, stained with 1 mM uranyl acetate. The insets for both (a) and (b) depict photographs of the two nanocomposites as dried powders. (c) Normalized Au 4f XPS spectra comparing the compositional profiles of nanocomposites fabricated in various conditions: (black line) Au@ChsNC-HR and (blue line) Au@ChsNC-LBL, with the

theoretical binding energy of metallic Au at 84.0 eV shown as the dotted line. The inset depicts the deconvolution of the Au@ChsNC-HR Au 4f XPS spectrum. (d) The deconvolution of the Au@ChsNC-HR Au 4f XPS spectrum found in (c).

This aggregation is consistent with the fact that ChsNCs feature a strongly positive surface charge, repulsing the positively charge PDDA-covered Au NPs. This is contrasted by the uniform distribution of Au NPs on CNCs using the same LBL method, since the CNCs in this case featured carboxylate anionic functionalities on their surface.[18]

Alternatively we used a one-pot deposition-precipitation technique, via hydrogen reduction (HR), in which the Au salt precursor was reduced by hydrogen gas *in situ* within a suspension of ChsNCs, inspired by work done to access Pd@CNCs.[17] As seen in Figure 2b and Figure S7, while the HR method created larger Au NPs (6.6 ± 1.8 nm), they were far less aggregated for Au@ChsNC-HR than the immobilized Au NPs found using the LBL method. Moreover, all Au NPs were located on the surface of ChsNCs, with no "free" Au NPs unattached to a ChsNC. We hypothesized that the carboxylate functionalities on the ChsNCs could promote a suitable coordination environment for Au salts, which were then subsequently reduced *in situ* into NPs, favoring good dispersity and interaction with the support.[58]

Along with the contrast in morphology created between the two fabrication procedures, the resulting Au species immobilized on ChsNCs from the two processes were also chemically dissimilar. X-ray photoelectron spectroscopy (XPS) was used to analyze the oxidation state of Au from both LBL and HR methods, as found in Figure 2c. The two

peaks in the normalized Au 4f high-resolution XPS spectra are the Au $4f_{5/2}$ and Au $4f_{7/2}$ spin-orbit split peaks. For the Au $4f_{7/2}$ binding energies of the Au@ChsNC-LBL seen in Figure 2c, the peak was at 83.1 eV, which is a lower binding energy than the theoretical binding energy of metallic Au of 84.0 eV, marked by a dotted line in Figure 2c. This could be attributed to the lower cluster size of the Au being in a NP form, which has been reported by other groups, as well as electron transfer from the stabilizing carbonate ligand to the Au NP itself.[59, 60]

As for the Au4f spectrum of Au@ChsNC-HR (black line, Figure 2c), the Au $4f_{7/2}$ peak was at a higher binding energy than 84.0 eV. Deconvolution of this peak (Figure 2d) revealed it enveloped two sub-peaks at 83.0 and 84.9 eV, attributed to Au^0 and Au^I, respectively.[61, 62] XRD spectra further corroborated this observation of the partial reduction of Au using the HR method, contrary to the LBL method (Figure S8). No reflection planes for metallic Au were found in the Au@ChsNC-HR, while broad reflections at 38.1° and 44.3° in the Au@ChsNC-LBL material were indicative of the presence of elemental Au.[63, 64] This further validated the incomplete reduction of Au within the Au@ChsNC-HR material. The influence of pH during the HR reduction of Au on ChsNCs was investigated and is provided in the supplemental information (SI) section below Figure S9. Low pH conditions favoured the formation of Au^0, while at higher pH the formation of Au^I was evident.

<u>Catalytic reduction of 4-nitrophenol</u>

The catalytic performance of Au@ChsNC-LBL and Au@ChsNC-HR for the 4-nitrophenol reduction were evaluated by UV-vis spectroscopy (Figure 5).[65-67]

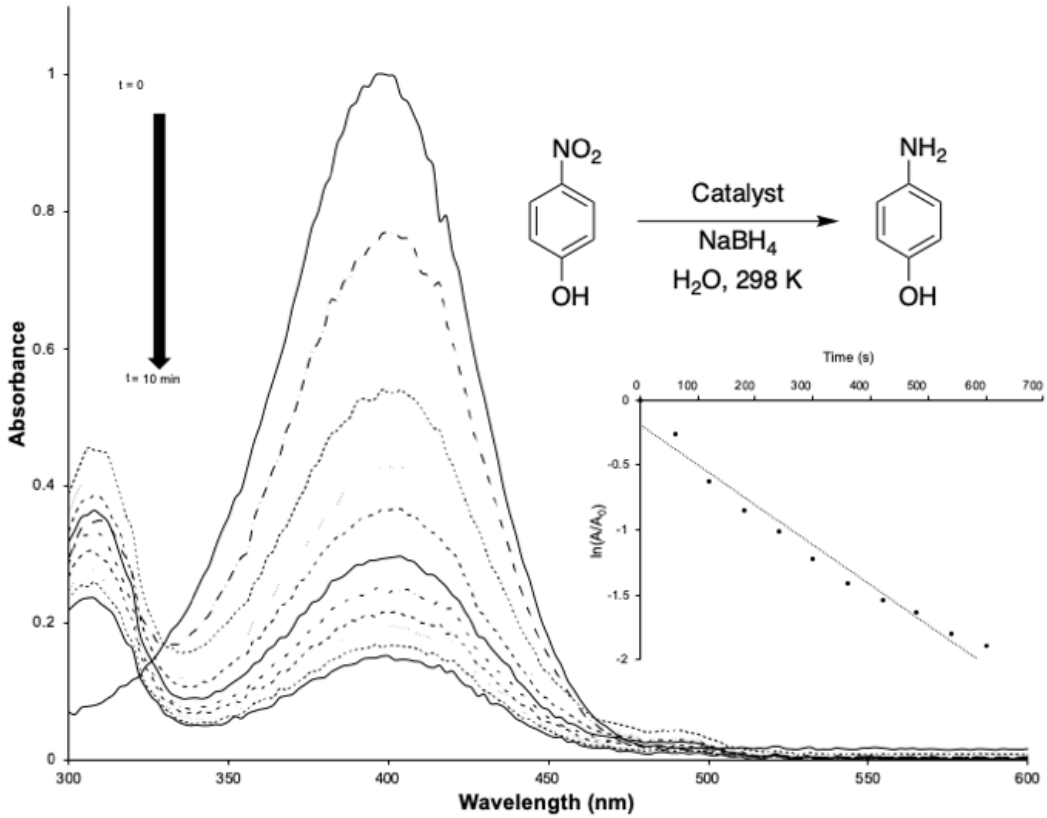

Figure 3. Representative time-dependant UV-Vis absorption spectra for the reduction of 4-nitrophenol to 4-aminophenol from 0 to 10 min using Au@ChsNC-LBL. The insets depict the reaction equation (top right) along with the plot of ln (A/A_0) vs. time (bottom right) depicting the pseudo-first order kinetics of the reaction

After addition of the catalyst to the reaction mixture, a decrease in the intensity at 400 nm from the 4-nitrophenolate anion was accompanied by a slight increase in absorption at 295 nm, corresponding to the absorption of 4-aminophenolate anion. The reaction with either catalyst system reached 99% completion within the first 10 min. All 4-nitrophenol

reduction reactions were done at room temperature (298 K) unless otherwise specified. The activation energies for Au@ChsNC-LBL and Au@ChsNC-HR were 28.4 and 36.7 kJ/mol, respectively, as calculated from the Arrhenius plots shown in Figure S10. Table 2 shows the calculated rate constants and turnover frequencies (TOFs) for various catalysts made in this work.

Table 2: Rate constants and turnover frequency values for the reduction of 4-nitrophenol to 4-aminophenol for various catalysts and supports.

Entry	Synthesis method	Catalyst Support	Au loading (%)	Rate Constant (s^{-1})	TOF (h^{-1})
1	3 nm Au NP	-	1	(2.04 ± 0.76) x 10-3	352 ± 139
2	HAuCl4	-	1	(3.36 ± 0.43) x 10-4	320 ± 18
3	LBL	ChsNC	0.2	(4.47 ± 0.73) x 10-4	616 ± 61
4	LBL	Bulk chitosan	1	(9.97 ± 2.4) x 10-5	41 ± 12
5	LBL	ChNC	1	(5.74 ± 0.20) x 10-4	153 ± 0.3
6	LBL	Bulk chitin	1	(3.55 ± 0.11) x 10-4	106 ± 1
7	HR	ChsNC	0.2	(4.75 ± 0.77) x 10-3	8557 ± 1117
8	HR	Bulk chitosan	0.2	(7.80 ± 2.0) x 10-5	152 ± 24

Firstly, free 3 nm carbonate-stabilized Au NPs – the one used in the LBL method - proved to be active in the catalytic reaction, serving as a positive control for the reaction conditions (entry **1**). The ability for *in situ* reduction of Au during the catalyst experiment is proven by testing $HAuCl_4$ as a catalyst (entry **2**), where $NaBH_4$ acts to reduce $HAuCl_4$ to metallic Au which serves as the catalyst site, as the 4-nitrophenol reduction reaction cannot proceed without an active metallic site for adsorption of substrates, illustrated by the Langmuir-Hinshelwood model.[68-70] The comparison between the performance of

Au@ChsNC-LBL and Au NPs supported on bulk chitosan revealed the importance of bringing chitosan down to the nanoscale. Au@ChsNC-LBL featured a TOF value over an order of magnitude higher than Au NPs supported by chitosan (entries **3** and **4**). This is also seen for chitin as well, in which Au supported on ChNCs has a higher TOF value (entry **5**) than Au supported on bulk chitin (entry **6**). It is also important to note that the ChsNCs support for Au NPs (entry **3**) outperformed the ChNCs support (entry **5**). A possible explanation lies in the fact that ChsNCs being positively charges overall, may interact favorably with borohydride anions and accelerate reaction accordingly. Furthermore, by comparing the two methods for producing catalysts on ChsNCs, the HR method (entry **7**) was superior to the LBL method with a TOF value (8557 h^{-1}) an order of magnitude greater than the LBL method (entry **3**, 616 h^{-1}). From prior characterization of the material, the HR method yielded a catalyst with a significant portion of the metal in the +1 redox state, likely stabilized by carboxylate functionalities on the surface of ChsNCs. These are presumably reduced *in situ* under the catalytic conditions to yield highly dispersed active sites. On the other hand, the LBL method results in aggregation of Au NPs present on the ChsNCs. This may explain the superior activity observed with the HR made nanocatalysts. We attempted XPS analysis post-catalysis, unfortunately too much noise inhibited valid understanding of the Au oxidation state. Finally, negative control tests without the catalyst substrate, along with reactions containing only ChsNCs, PDDA/ChsNCs and PDDA/ChNCs, yielded no observable conversion.

Au-ChsNC nanocatalysts exhibited superior catalytic activity compared to literature values for other Au-based catalysts immobilized on carbon-based supports (Table S2).

This nanocomposite system even outperformed Pd-based catalysts for the nitrophenol reduction. This assessment clearly depicts that through the combined characteristics of nanoscale dimensions and unique amine and carboxylate functionalities, ChsNCs are a viable, biomass-based support capable of outperforming the current CNC-based supports popularly utilized.

By using the 4-nitrophenol model reaction as a framework for demonstrating catalytic ability of these nanomaterials, we have concluded the efficacy of using nanoscale chitin and chitosan over their bulk counterparts. Moreover, we establish the ability of chitosan as a much better support for Au NPs in lieu of chitin, as well as develop a one-pot synthesis to immobilize Au onto the ChsNC structure with control of the Au oxidation state. From this framework, we studied the activity of these nanocatalysts for another important chemical transformation.

<u>A^3 Coupling Catalysis</u>

The A^3 coupling reaction is an atom-economical reaction for the multi-component synthesis of propargylamines.[71] It serves as alternative to the less sustainable reaction of using stoichiometric quantities of organometallic reagents such as butyllithium to activate the highly acidic terminal hydrogen of an alkynyl to form a metal acetylide, before subsequent addition to an imine.[72, 73] Much work has been performed to understand its mechanism, along with developing more effective catalysts for this reaction in terms of TOF, stability, and recyclability.[74] More specifically, the usage of Au as a transition metal catalyst has been studied extensively within the field.[75] Both metallic Au NPs[74] as well as

Au salts in the form of Au^{I}/Au^{III} have the ability to catalyze this reaction.[71, 76, 77] For example, Li and coworkers have shown that Au^{I} salts are effective catalyst for the synthesis of propargylamines in water.[78] Work has also been done on using biomaterials such as CNCs to support Au catalysts for A^3 coupling, albeit with lower activity than their homogenous counterparts.[79] Spurred by the heightened catalytic ability of Au@ChsNC-HR, where the highly dispersed gold exists as Au^0 and Au^{I}, we explored the ability of this nanomaterial to catalyze the A^3 coupling reaction.

In a standard procedure, we used model substrates, benzaldehyde, piperidine, and phenylacetylene, keeping the benzaldehyde as the limiting reagent in order to favour formation of the imine intermediate. From Table 3, it can be seen that by using the free carbonate-stabilized Au NPs, negligible amounts of product was formed, evidencing that metallic Au may not play a major role as the active catalyst in the A^3 coupling reaction (entry **9**). In contrast to this, using the $HAuCl_4$ salt is seen to have full conversion to the proparglymine product in 24 h (entry **10**). The inability for Au^0 to catalyze the reaction is further seen by using Au@ChsNC-LBL (8%, entry **11**), which was confirmed previously to feature pure Au^0. In contrast, substantial conversion and yield can be seen using Au@ChsNC-HR with only 0.1 mol% Au loading (91%, entry **12**). By increasing the Au loading to 0.5 mol% Au, full conversion was reported (entry **13**). Lower yields of 69% and 40% were reported at 6 h for 0.5 mol% (entry **14**) and 0.1 mol% (entry **15**) Au loading, respectively. The effects of temperature were examined as well in which >90% yield was achieved at 50 °C (entry **16**). However, when the temperature is increased to 100 °C, a substantial decrease in yield is seen (56%, entry **17**). This may be caused by potential

degradation of the catalyst at this temperature, which would inhibit the formation of the final product.

Table 3. A^3 coupling reaction table. All reactions listed are done using 1 mmol benzaldehyde, 1.2 mmol piperidine, and 1.5 mmol phenylacetylene, with no solvent. Yield was determined through ^{1}H NMR. [a]Reaction done using water as the solvent.

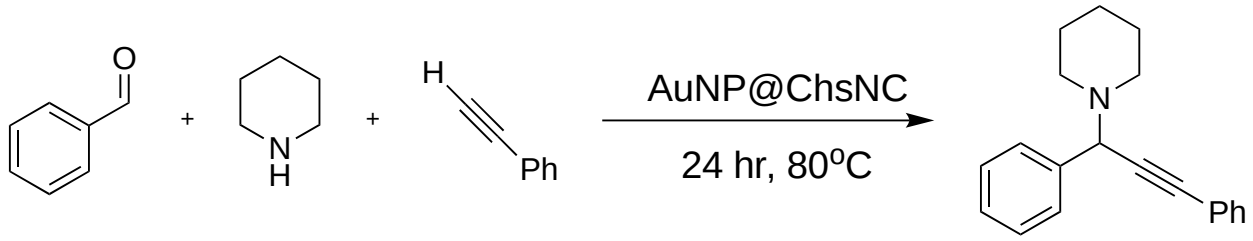

Entry	Synthesis method	Catalyst Support	Au loading (%)	Temperature (°C)	Time (h)	Yield (%)
9[a]	3 nm Au NP	-	1	80	24	2
10[a]	HAuCl4	-	1	80	24	>99
11	LBL	ChsNC	0.1	70	24	8
12	HR	ChsNC	0.1	70	24	91
13	HR	ChsNC	0.5	70	24	>99
14	HR	ChsNC	0.5	70	6	69
15	HR	ChsNC	0.1	70	6	40
16	HR	ChsNC	0.5	50	24	92
17	HR	ChsNC	0.5	100	24	56

Conclusions

In this work, we present the first method to produce carboxylated ChsNCs from bulk chitin. Using ammonium persulfate as a mild oxidant, cleavage of the chitin amorphous regions with concurrent oxidation of the C6 alcohol groups leads to the formation of carboxylated ChNCs. Moreover, through a facile procedure using $NaBH_4$ in alkaline conditions to limit

uncontrolled depolymerization, deacetylation of ChNCs occurs to produce ChsNCs with high DDA, retention of the nanorod structure and surface carboxylic acid functionality. Two different methods were used to create Au-immobilized ChsNC catalysts in which the composition and topography of these nanomaterials can be directly altered through the reaction conditions. The catalytic properties of the nanomaterial were then investigated in the reduction of 4-nitrophenol and the A^3 coupling reaction. We have shown that nanoscale chitin and chitosan have a clear advantage in activity over bulk chitin and chitosan as support materials for heterogenous catalysis. A highly dispersed dual Au^I/Au^0 nanocatalyst (Au@ChsNC-HR) fabricated by direct hydrogen reduction of $HAuCl_4$ on ChsNC showed significant activity for both model catalyst reactions. To the best of our knowledge, the Au@ChsNC-HR nanocatalyst exhibits the highest reported TOF for the classical 4-nitrophenol reduction reaction on carbon based-supports. From this work, we hope to show the potential of deriving high value products from chitinous waste streams obtained from the seafood industry, as well as exhibit the unique physicochemical properties of ChsNCs conferred by the both different functional groups and its nanorod-structure. This work provides a prospective of ChsNCs as a new bio-nanomaterial that can compete with and possibly overcome CNCs in terms of applicability and efficacy.

ASSOCIATED CONTENT

Supporting Information

The supporting information is available free of charge on the ACS Publications website.

Experimental procedures depicting the syntheses of ChNC and ChsNC and their scale-up, fabrication methods for Au@ChsNC, standard catalytic reaction protocols, and additional characterization information including AFM, FTIR peak assignments, UV-Vis spectra, DLS, TEM, XRD, XPS, as well as a table comparing rate constant and turnover frequency of the 4-nitrophenol reaction obtained in this study with other works (PDF).

Author Information

Corresponding Authors

*Email: audrey.moores@mcgill.ca

*Email: edmond.lam@cnrc-nrc.gc.ca

Author contributions

All authors have given final approval to the final version of the manuscript.

Notes

The authors declare no competing financial interest

Acknowledgements

We thank the Natural Science and Engineering Research Council of Canada (NSERC) Discovery Grant and Discovery Accelerator Supplement, the Canada Foundation for Innovation (CFI), the National Research Council (NRC) New Beginnings Initiative Ideation fund, the Centre for Green Chemistry and Catalysis (CGCC), the National Research Council Canada (NRC), and McGill University for their financial support. We thank the Facility for Electron Microscopy Research of McGill University for help in data collection. We thank the MC^2 facility at McGill University for help in acquiring the FTIR and UV-Vis spectra. Specifically, we thank Dr. Hatem Titi from the MC^2 facility for help in acquiring PXRD spectra along with fruitful scientific discussion.

References

1. Dufresne, A., *Mater. Today* Nanocellulose: a new ageless bionanomaterial. **2013,** *16*, 220-227.
2. Andresen, M.; Stenstad, P.; Møretrø, T.; Langsrud, S.; Syverud, K.; Johansson, L.-S.; Stenius, P., *Biomacromolecules* Nonleaching Antimicrobial Films Prepared from Surface-Modified Microfibrillated Cellulose. **2007,** *8*, 2149-2155.
3. Thomas, B.; Raj, M. C.; B, A. K.; H, R. M.; Joy, J.; Moores, A.; Drisko, G. L.; Sanchez, C., *Chem. Rev.* Nanocellulose, a Versatile Green Platform: From Biosources to Materials and Their Applications. **2018,** *118*, 11575-11625.
4. Xu, Q.; Gao, Y.; Qin, M.; Wu, K.; Fu, Y.; Zhao, J., *Int. J. Biol. Macromol.* Nanocrystalline cellulose from aspen kraft pulp and its application in deinked pulp. **2013,** *60*, 241-247.
5. Shojaeiarani, J.; Bajwa, D.; Shirzadifar, A., *Carbohydr. Polym.* A review on cellulose nanocrystals as promising biocompounds for the synthesis of nanocomposite hydrogels. **2019,** *216*, 247-259.
6. Cunha, A. G.; Mougel, J.-B.; Cathala, B.; Berglund, L. A.; Capron, I., *Langmuir* Preparation of Double Pickering Emulsions Stabilized by Chemically Tailored Nanocelluloses. **2014,** *30*, 9327-9335.
7. Jackson, J. K.; Letchford, K.; Wasserman, B. Z.; Ye, L.; Hamad, W. Y.; Burt, H. M., *Int J Nanomedicine* The use of nanocrystalline cellulose for the binding and controlled release of drugs. **2011,** *6*, 321-330.
8. Zhou, Z.; Lu, C.; Wu, X.; Zhang, X., *RSC Adv.* Cellulose nanocrystals as a novel support for CuO nanoparticles catalysts: facile synthesis and their application to 4-nitrophenol reduction. **2013,** *3*, 26066-26073.
9. Kaushik, M.; Basu, K.; Benoit, C.; Cirtiu, C. M.; Vali, H.; Moores, A., *J. Am. Chem. Soc.* Cellulose Nanocrystals as Chiral Inducers: Enantioselective Catalysis and Transmission Electron Microscopy 3D Characterization. **2015,** *137*, 6124-6127.
10. Tang, J.; Shi, Z.; Berry, R. M.; Tam, K. C., *Ind. Eng. Chem. Res.* Mussel-Inspired Green Metallization of Silver Nanoparticles on Cellulose Nanocrystals and Their Enhanced Catalytic Reduction of 4-Nitrophenol in the Presence of β-Cyclodextrin. **2015,** *54*, 3299-3308.
11. Yan, W.; Chen, C.; Wang, L.; Zhang, D.; Li, A.-J.; Yao, Z.; Shi, L.-Y., *Carbohydr. Polym.* Facile and green synthesis of cellulose nanocrystal-supported gold nanoparticles with superior catalytic activity. **2016,** *140*, 66-73.
12. George, J.; Sabapathi, S. N., *Nanotechnol Sci Appl* Cellulose nanocrystals: synthesis, functional properties, and applications. **2015,** *8*, 45-54.
13. Rezayat, M.; Blundell, R. K.; Camp, J. E.; Walsh, D. A.; Thielemans, W., *ACS Sustain. Chem. Eng.* Green One-Step Synthesis of Catalytically Active Palladium Nanoparticles Supported on Cellulose Nanocrystals. **2014,** *2*, 1241-1250.
14. Kaushik, M.; Moores, A., *Green Chem.* Review: nanocelluloses as versatile supports for metal nanoparticles and their applications in catalysis. **2016,** *18*, 622-637.
15. Kaushik, M.; Friedman, H. M.; Bateman, M.; Moores, A., *RSC Adv.* Cellulose nanocrystals as non-innocent supports for the synthesis of ruthenium nanoparticles and their application to arene hydrogenation. **2015,** *5*, 53207-53210.

16. Kaushik, M.; Li, A. Y.; Hudson, R.; Masnadi, M.; Li, C.-J.; Moores, A., *Green Chem.* Reversing aggregation: direct synthesis of nanocatalysts from bulk metal. Cellulose nanocrystals as active support to access efficient hydrogenation silver nanocatalysts. **2016,** *18*, 129-133.
17. Cirtiu, C. M.; Dunlop-Brière, A. F.; Moores, A., *Green Chem.* Cellulose nanocrystallites as an efficient support for nanoparticles of palladium: application for catalytic hydrogenation and Heck coupling under mild conditions. **2011,** *13*, 288-291.
18. Lam, E.; Hrapovic, S.; Majid, E.; Chong, J. H.; Luong, J. H. T., *Nanoscale* Catalysis using gold nanoparticles decorated on nanocrystalline cellulose. **2012,** *4*, 997-1002.
19. Kim, S.-K., *Chitin, chitosan, oligosaccharides and their derivatives: biological activities and applications*. CRC Press: 2010.
20. Gopalan Nair, K.; Dufresne, A., *Biomacromolecules* Crab Shell Chitin Whisker Reinforced Natural Rubber Nanocomposites. 1. Processing and Swelling Behavior. **2003,** *4*, 657-665.
21. MacLeod, J. A.; Kuo, S.; Gallant, T. L.; Grimmett, M., *Can. J. Soil Sci.* Seafood processing wastes as nutrient sources for crop production. **2006,** *86*, 631-640.
22. Yan, N.; Chen, X., *Nature* Sustainability: Don't waste seafood waste. **2015,** *524*, 155-157.
23. Yang, H.; Gözaydın, G.; Nasaruddin, R. R.; Har, J. R. G.; Chen, X.; Wang, X.; Yan, N., *ACS Sustain. Chem. Eng.* Toward the Shell Biorefinery: Processing Crustacean Shell Waste Using Hot Water and Carbonic Acid. **2019,** *7*, 5532-5542.
24. Shahidi, F.; Arachchi, J. K. V.; Jeon, Y.-J., *Trends Food Sci. Technol.* Food applications of chitin and chitosans. **1999,** *10*, 37-51.
25. Park, B. K.; Kim, M.-M., *Int. J. Mol. Sci.* Applications of chitin and its derivatives in biological medicine. **2010,** *11*, 5152-5164.
26. Jayakumar, R.; Menon, D.; Manzoor, K.; Nair, S. V.; Tamura, H., *Carbohydr. Polym.* Biomedical applications of chitin and chitosan based nanomaterials—A short review. **2010,** *82*, 227-232.
27. Margoutidis, G.; Parsons, V. H.; Bottaro, C. S.; Yan, N.; Kerton, F. M., *ACS Sustain. Chem. Eng.* Mechanochemical Amorphization of α-Chitin and Conversion into Oligomers of N-Acetyl-d-glucosamine. **2018,** *6*, 1662-1669.
28. Di Nardo, T.; Hadad, C.; Nguyen Van Nhien, A.; Moores, A., *Green Chem.* Synthesis of high molecular weight chitosan from chitin by mechanochemistry and aging. **2019,** *21*, 3276-3285.
29. Zhou, J.; Dong, Z.; Yang, H.; Shi, Z.; Zhou, X.; Li, R., *Appl. Surf. Sci.* Pd immobilized on magnetic chitosan as a heterogeneous catalyst for acetalization and hydrogenation reactions. **2013,** *279*, 360-366.
30. Qiu, Y.; Ma, Z.; Hu, P., *J. Mater. Chem. A* Environmentally benign magnetic chitosan/Fe3O4 composites as reductant and stabilizer for anchoring Au NPs and their catalytic reduction of 4-nitrophenol. **2014,** *2*, 13471-13478.
31. Wei, D.; Ye, Y.; Jia, X.; Yuan, C.; Qian, W., *Carbohydr. Res.* Chitosan as an active support for assembly of metal nanoparticles and application of the resultant bioconjugates in catalysis. **2010,** *345*, 74-81.

32. Primo, A.; Quignard, F., *Chem. Commun.* Chitosan as efficient porous support for dispersion of highly active gold nanoparticles: design of hybrid catalyst for carbon–carbon bond formation. **2010,** *46*, 5593-5595.
33. Fan, Y.; Saito, T.; Isogai, A., *Biomacromolecules* Chitin Nanocrystals Prepared by TEMPO-Mediated Oxidation of α-Chitin. **2008,** *9*, 192-198.
34. Goodrich, J. D.; Winter, W. T., *Biomacromolecules* α-Chitin Nanocrystals Prepared from Shrimp Shells and Their Specific Surface Area Measurement. **2007,** *8*, 252-257.
35. Fan, Y.; Saito, T.; Isogai, A., *Biomacromolecules* Preparation of Chitin Nanofibers from Squid Pen β-Chitin by Simple Mechanical Treatment under Acid Conditions. **2008,** *9*, 1919-1923.
36. Luong, J. H.; Lam, E.; Leung, C. W.; Hrapovic, S.; Male, K. B., Chitin Nanocrystals and Process for Preparation Thereof. US Patent: 2016.
37. Ma, Q.; Pang, K.; Wang, K.; Huang, S.; Ding, B.; Duan, Y.; Zhang, J., *Carbohydr. Polym.* Ultrafine and carboxylated β-chitin nanofibers prepared from squid pen and its transparent hydrogels. **2019,** *211*, 118-123.
38. Oun, A. A.; Rhim, J.-W., *Carbohydr. Polym.* Effect of oxidized chitin nanocrystals isolated by ammonium persulfate method on the properties of carboxymethyl cellulose-based films. **2017,** *175*, 712-720.
39. Oun, A. A.; Rhim, J.-W., *Carbohydr. Polym.* Effect of isolation methods of chitin nanocrystals on the properties of chitin-silver hybrid nanoparticles. **2018,** *197*, 349-358.
40. Haruta, M., *Chem. Rec.* When Gold Is Not Noble: Catalysis by Nanoparticles. **2003,** *3*, 75-87.
41. Lu, P.; Hsieh, Y.-L., *Carbohydr. Polym.* Preparation and characterization of cellulose nanocrystals from rice straw. **2012,** *87*, 564-573.
42. Hon, D. N.-S.; Shiraishi, N., *Wood and cellulosic chemistry, revised, and expanded*. CRC press: 2000.
43. Leung, A. C. W.; Hrapovic, S.; Lam, E.; Liu, Y.; Male, K. B.; Mahmoud, K. A.; Luong, J. H. T., *Small* Characteristics and Properties of Carboxylated Cellulose Nanocrystals Prepared from a Novel One-Step Procedure. **2011,** *7*, 302-305.
44. Wada, M.; Saito, Y., *J. Polym. Sci. Pol. Phys.* Lateral thermal expansion of chitin crystals. **2001,** *39*, 168-174.
45. Feng, F.; Liu, Y.; Hu, K., *Carbohydr. Res.* Influence of alkali-freezing treatment on the solid state structure of chitin. **2004,** *339*, 2321-2324.
46. Li, J.; Revol, J. F.; Marchessault, R. H., *J. Appl. Polym.* Effect of degree of deacetylation of chitin on the properties of chitin crystallites. **1997,** *65*, 373-380.
47. Lavall, R. L.; Assis, O. B. G.; Campana-Filho, S. P., *Bioresour. Technol.* β-Chitin from the pens of Loligo sp.: Extraction and characterization. **2007,** *98*, 2465-2472.
48. Heath, L.; Zhu, L.; Thielemans, W., *ChemSusChem* Chitin Nanowhisker Aerogels. **2013,** *6*, 537-544.
49. Sjostrom, E., *Wood chemistry: fundamentals and applications*. Gulf professional publishing: 1993.
50. Batista, I.; Roberts, G. A. F., *Makromol. Chem.* A novel, facile technique for deacetylating chitin. **1990,** *191*, 429-434.

51. Shigemasa, Y.; Matsuura, H.; Sashiwa, H.; Saimoto, H., *Int. J. Biol. Macromol.* Evaluation of different absorbance ratios from infrared spectroscopy for analyzing the degree of deacetylation in chitin. **1996,** *18*, 237-242.
52. Lertwattanaseri, T.; Ichikawa, N.; Mizoguchi, T.; Tanaka, Y.; Chirachanchai, S., *Carbohydr. Res.* Microwave technique for efficient deacetylation of chitin nanowhiskers to a chitosan nanoscaffold. **2009,** *344*, 331-335.
53. Zhang, Y.; Xue, C.; Xue, Y.; Gao, R.; Zhang, X., *Carbohydr. Res.* Determination of the degree of deacetylation of chitin and chitosan by X-ray powder diffraction. **2005,** *340*, 1914-1917.
54. Clark, G. L.; Smith, A. F., *J. Phys. Chem.* X-ray Diffraction Studies of Chitin, Chitosan, and Derivatives. **2002,** *40*, 863-879.
55. Liu, H.; Wang, C.; Zou, S.; Wei, Z.; Tong, Z., *Langmuir* Simple, Reversible Emulsion System Switched by pH on the Basis of Chitosan without Any Hydrophobic Modification. **2012,** *28*, 11017-11024.
56. Liz-Marzán, L. M., *Langmuir* Tailoring Surface Plasmons through the Morphology and Assembly of Metal Nanoparticles. **2006,** *22*, 32-41.
57. Moores, A.; Goettmann, F., *New J. Chem.* The plasmon band in noble metal nanoparticles: an introduction to theory and applications. **2006,** *30*, 1121-1132.
58. Zhao, P.; Li, N.; Astruc, D., *Coord. Chem. Rev.* State of the art in gold nanoparticle synthesis. **2013,** *257*, 638-665.
59. Konova, P.; Naydenov, A.; Venkov, C.; Mehandjiev, D.; Andreeva, D.; Tabakova, T., *J. Mol. Catal. A: Chem.* Activity and deactivation of Au/TiO2 catalyst in CO oxidation. **2004,** *213*, 235-240.
60. Arrii, S.; Morfin, F.; Renouprez, A. J.; Rousset, J. L., *J. Am. Chem. Soc.* Oxidation of CO on Gold Supported Catalysts Prepared by Laser Vaporization: Direct Evidence of Support Contribution. **2004,** *126*, 1199-1205.
61. Molnár, Á., *Coord. Chem. Rev.* The use of chitosan-based metal catalysts in organic transformations. **2019,** *388*, 126-171.
62. Sun, C.; Qu, R.; Chen, H.; Ji, C.; Wang, C.; Sun, Y.; Wang, B., *Carbohydr. Res.* Degradation behavior of chitosan chains in the ‘green’ synthesis of gold nanoparticles. **2008,** *343*, 2595-2599.
63. Tsunoyama, H.; Sakurai, H.; Ichikuni, N.; Negishi, Y.; Tsukuda, T., *Langmuir* Colloidal Gold Nanoparticles as Catalyst for Carbon−Carbon Bond Formation: Application to Aerobic Homocoupling of Phenylboronic Acid in Water. **2004,** *20*, 11293-11296.
64. Chen, Y.; Gu, X.; Nie, C.-G.; Jiang, Z.-Y.; Xie, Z.-X.; Lin, C.-J., *Chem. Commun.* Shape controlled growth of gold nanoparticles by a solution synthesis. **2005**, 4181-4183.
65. Li, J.; Liu, C.-y.; Liu, Y., *J. Mater. Chem.* Au/graphene hydrogel: synthesis, characterization and its use for catalytic reduction of 4-nitrophenol. **2012,** *22*, 8426-8430.
66. Zeng, J.; Zhang, Q.; Chen, J.; Xia, Y., *Nano Lett.* A Comparison Study of the Catalytic Properties of Au-Based Nanocages, Nanoboxes, and Nanoparticles. **2010,** *10*, 30-35.

67. Lee, J.; Park, J. C.; Song, H., *Adv. Mater.* A Nanoreactor Framework of a Au@SiO2 Yolk/Shell Structure for Catalytic Reduction of p-Nitrophenol. **2008,** *20*, 1523-1528.
68. Pandey, S.; Mishra, S. B., *Carbohydr. Polym.* Catalytic reduction of p-nitrophenol by using platinum nanoparticles stabilised by guar gum. **2014,** *113*, 525-531.
69. Zhao, P.; Feng, X.; Huang, D.; Yang, G.; Astruc, D., *Coord. Chem. Rev.* Basic concepts and recent advances in nitrophenol reduction by gold- and other transition metal nanoparticles. **2015,** *287*, 114-136.
70. Rodrigues, C. S. D.; Soares, O. S. G. P.; Pinho, M. T.; Pereira, M. F. R.; Madeira, L. M., *Appl. Catal., B* p-Nitrophenol degradation by heterogeneous Fenton's oxidation over activated carbon-based catalysts. **2017,** *219*, 109-122.
71. Peshkov, V. A.; Pereshivko, O. P.; Van der Eycken, E. V., *Chem. Soc. Rev.* A walk around the A3-coupling. **2012,** *41*, 3790-3807.
72. Ma, Y.; Lobkovsky, E.; Collum, D. B., *J. Org. Chem.* BF3-Mediated Additions of Organolithiums to Ketimines: X-ray Crystal Structures of BF3−Ketimine Complexes. **2005,** *70*, 2335-2337.
73. Aubrecht, K. B.; Winemiller, M. D.; Collum, D. B., *J. Am. Chem. Soc.* BF3-Mediated Addition of Lithium Phenylacetylide to an Imine: Correlations of Structures and Reactivities. BF3·R3N Derivatives as Substitutes for BF3·Et2O. **2000,** *122*, 11084-11089.
74. Nasrollahzadeh, M.; Sajjadi, M.; Ghorbannezhad, F.; Sajadi, S. M., *Chem. Rec.* A Review on Recent Advances in the Application of Nanocatalysts in A3 Coupling Reactions. **2018,** *18*, 1409-1473.
75. Soengas, R.; Navarro, Y.; Iglesias, M. J.; López-Ortiz, F., *Molecules (Basel, Switzerland)* Immobilized Gold Nanoparticles Prepared from Gold(III)-Containing Ionic Liquids on Silica: Application to the Sustainable Synthesis of Propargylamines. **2018,** *23*, 2975.
76. Cheng, M.; Zhang, Q.; Hu, X.-Y.; Li, B.-G.; Ji, J.-X.; Chan, A. S. C., *Adv. Synth. Catal.* Gold-Catalyzed Direct Intermolecular Coupling of Ketones, Secondary Amines, and Alkynes: A Facile and Versatile Access to Propargylic Amines Containing a Quaternary Carbon Center. **2011,** *353*, 1274-1278.
77. Shore, G.; Yoo, W.-J.; Li, C.-J.; Organ, M. G., *Chem. Eur. J.* Propargyl Amine Synthesis Catalysed by Gold and Copper Thin Films by Using Microwave-Assisted Continuous-Flow Organic Synthesis (MACOS). **2010,** *16*, 126-133.
78. Wei, C.; Li, C.-J., *J. Am. Chem. Soc.* A Highly Efficient Three-Component Coupling of Aldehyde, Alkyne, and Amines via C−H Activation Catalyzed by Gold in Water. **2003,** *125*, 9584-9585.
79. Huang, J.-L.; Gray, D. G.; Li, C.-J., *Beilstein J. Org. Chem.* A3-Coupling catalyzed by robust Au nanoparticles covalently bonded to HS-functionalized cellulose nanocrystalline films. **2013,** *9*, 1388-1396.

p

Table of Contents/Abstract Graphic